

“Darker-than-Black” PbS Quantum Dots: Enhancing Optical Absorption of Colloidal Semiconductor Nanocrystals via Short Conjugated Ligands

Carlo Giansante,^{*,†,‡} Ivan Infante,^{⊥,||} Eduardo Fabiano,^{†,‡} Roberto Grisorio,[#] Gian Paolo Suranna,[#] and Giuseppe Gigli^{§,¶}

[†]Center for Biomolecular Nanotechnologies @UNILE, Istituto Italiano di Tecnologia, via Barsanti 1, 73010 Arnesano, Lecce, Italy

[‡]NNL-CNR Istituto di Nanoscienze, via per Arnesano, 73100 Lecce, Lecce, Italy

[⊥]Kimika Fakultatea, Euskal Herriko Unibertsitatea and Donostia International Physics Center (DIPC), CP1072, 20080 San Sebastian, Spain

^{||}Department of Theoretical Chemistry, Faculty of Sciences, Vrije Universiteit Amsterdam, De Boelelaan 1083, 1081 HV Amsterdam, The Netherlands

[#]DICATECh - Dipartimento di Ingegneria Civile, Ambientale, del Territorio, Edile e di Chimica, Politecnico di Bari, via Orabona 4, 70125 Bari, Italy

[§]Dipartimento di Matematica e Fisica ‘E. De Giorgi’, Università del Salento, via per Arnesano, 73100 Lecce, Lecce, Italy

[¶]Istituto di Metodologie Inorganiche e dei Plasmi (I.M.I.P), Via Amendola 122/D, 70126 Bari, Italy

S Supporting Information

ABSTRACT: Colloidal quantum dots (QDs) stand among the most attractive light-harvesting materials to be exploited for solution-processed optoelectronic applications. To this aim, quantitative replacement of the bulky electrically insulating ligands at the QD surface coming from the synthetic procedure is mandatory. Here we present a conceptually novel approach to design light-harvesting nanomaterials demonstrating that QD surface modification with suitable short conjugated organic molecules permits us to drastically enhance light absorption of QDs, while preserving good long-term colloidal stability. Indeed, rational design of the pendant and anchoring moieties, which constitute the replacing ligand framework leads to a broadband increase of the optical absorbance larger than 300% for colloidal PbS QDs also at high energies (>3.1 eV), which could not be predicted by using formalisms derived from effective medium theory. We attribute such a drastic absorbance increase to ground-state ligand/QD orbital mixing, as inferred by density functional theory calculations; in addition, our findings suggest that the optical band gap reduction commonly observed for PbS QD solids treated with thiol-terminating ligands can be prevalently ascribed to 3p orbitals localized on anchoring sulfur atoms, which mix with the highest occupied states of the QDs. More broadly, we provide evidence that organic ligands and inorganic cores are inherently electronically coupled materials thus yielding peculiar chemical species (the colloidal QDs themselves), which display arising (opto)electronic properties that cannot be merely described as the sum of those of the ligand and core components.



INTRODUCTION

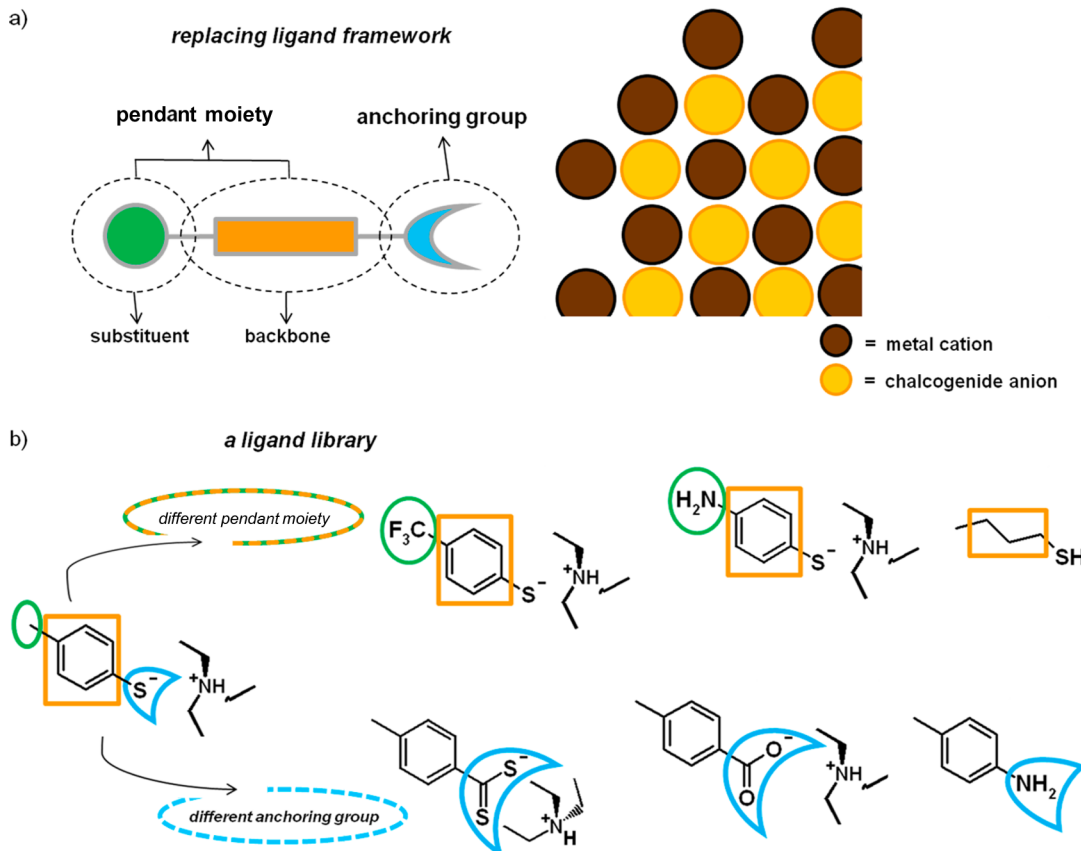
Colloidal semiconductor quantum dots (QDs) are particularly attractive as light-harvesting materials for cost-effective optoelectronic applications due to their tunable bandgap, large absorption coefficients, and compatibility with liquid-phase processing.¹ In most cases, such solution processability is guaranteed by organic ligands, which are already introduced during QD synthetic procedures to control nucleation and growth and to remove unsaturated valences;² however, these pristine ligands are generally electrically insulating long-chain aliphatic compounds and their postsynthesis replacement with shorter molecules is thus essential for QD integration in efficient optoelectronic devices.³ Indeed, the impact of ligands at the QD surface on optoelectronic properties has been widely

experimentally⁴ and computationally⁵ investigated. Here we show that QD surface modification with short conjugated ligands can be exploited to enhance solar-light absorption of colloidal QDs across the entire UV-vis-NIR spectral range, while preserving good long-term colloidal stability. We demonstrate that tailoring the pendant and anchoring moieties, which constitute the replacing ligand framework, permits us to tune such an optical absorption increase above 300%, also at high energies (>3.1 eV), for which it has been previously found that (molar) absorption coefficient is not affected by quantum confinement but scales with QD volume.^{6–9}

Received: October 25, 2014

Published: January 9, 2015

Scheme 1. (a) Scheme of the Replacing Ligand Framework Comprising an Anchoring Group and a Pendant Moiety, the Latter Constituted by a Backbone That Can Be Further Functionalized with Chosen Substituents^a and (b) Library of Here Employed Replacing Ligands, Which Bear Conjugated or Saturated Backbone (Orange Rectangles) Further Functionalized with Electron-Donating or -Accepting Substituents (Green Ovals) and Differ in the Nature and Bonding Mode of the Anchoring Group (Highlighted in Cyan)^b



^aSuch ligands are added to solutions of as-synthesized colloidal QDs. ^bNote that weak acidic character of AlSH prevents its deprotonation with triethylamine (Et_3N).

Organic ligands at the nanocrystal surface generally comprise (i) an anchoring group, which is commonly a Lewis base that coordinates the metal sites at the QD surface and removes unsaturated valences, and (ii) a pendant moiety, which mediates QD interactions with the surroundings and ensures QD colloidal stability (see Scheme 1). The colloidal stability, which we pursued in this work with short conjugated ligands, has a prominent role in the evaluation of the surface modification effects on QD photophysical properties, permitting the study of isolated QDs free-standing in solution-phase. This has been however a strong limitation in the case of lead-chalcogenide QDs due to their propensity to undergo oxidation,¹⁰ coalescence,¹¹ and aggregation upon the addition of small molecules as replacing ligands. As a consequence, pristine ligand replacement was prevalently carried out in solid phase,^{12–15} which prevents complete access of the replacing ligands to the QD surface and limits the investigation of the ligand/QD interface that may be hindered by concomitant inter-QD interactions. In order to overcome the limitations of the solid-phase ligand exchange, we have recently proposed a PbS QD surface modification strategy in solution phase that guarantees complete replacement of bulky pristine oleate ligands with short *p*-methylbenzenethiolate ligands, while preserving good long-term colloidal stability in chlorinated solvents that are commonly used for the solution-based

deposition of QDs into smooth dense-packed thin films;^{16,17} moreover, the good solubility of both ligands and QDs permits precise control of their concentrations in a closed system, which may instead be hampered by filtering¹⁸ or phase transfer¹⁹ of ligand-exchanged QD solutions. Here we further exploit such a solution-phase surface modification approach to describe the effects of replacing ligands on the optical absorption properties of colloidal QDs. We have thus employed the *p*-methylbenzenethiolate ligand (henceforth referred to as ArS^- , which has been prepared by deprotonating the thiol group in the presence of triethylamine, Et_3N)^{20,21} as a framework, which allows systematic modification of the replacing ligand subunits, namely, the pendant and the anchoring groups (as schematically shown in Scheme 1a). Indeed, we investigated the role of the pendant moiety by exploiting thiolate-terminated ligands while introducing in para position of the benzene ring an electron-accepting substituent (such as the trifluoromethyl group in $\text{A}-\text{ArS}^-/\text{Et}_3\text{NH}^+$ ionic couple) or an electron-donating substituent (as the amino group in $\text{D}-\text{ArS}^-/\text{Et}_3\text{NH}^+$ ionic couple) and comparing the effect of the conjugated backbone with that of a saturated analog (AlSH, which is a weaker acid than Et_3NH^+ , thus deprotonation of aliphatic thiols with Et_3N is prevented).^{20,21} We have also introduced different anchoring groups on the *p*-methylbenzene moiety, which differ in their chemical nature (S-, O-, and N-

terminated binding groups) and bonding mode (mono- and bidentate coordination geometries), namely, dithioate (ArCS_2^- , synthesized as Et_3NH^+ ionic couple), carboxylate (ArCO_2^- , prepared as Et_3NH^+ ionic couple), and amine (ArNH_2), in order to elucidate the role exerted by the binding moiety on the optical absorption properties of colloidal QDs. The ligand library used in this work is shown in Scheme 1b.

In this work, we exploit such rational design of the pendant and anchoring moieties, which constitute the replacing ligand framework, to describe and explain the ligand effect on the optical absorption properties of colloidal QDs. We observe a broadband enhancement of the optical absorption of colloidal PbS QDs induced by conjugated thiolate-terminated ligands, which can be tuned above 300% and is maximized for small QDs in virtue of their large surface-to-volume ratio. Our findings disclose the possibility of increasing the absorption coefficient of colloidal QDs also at energies far from the band gap (>3.1 eV), despite previous reports of size independence of the absorption coefficient in this spectral region.^{6–9} We present density functional theory calculations describing the investigated ligand/QD systems and their ground-state orbital mixing, which is at the basis of the observed enhancement of optical absorption otherwise indescribable as the mere sum of the properties of ligand and QD components. Here we thus provide a novel path in the design of light-harvesting nanomaterials, which could be applied in solution-processed photovoltaic and photodetection applications.

EXPERIMENTAL SECTION

Materials. All chemicals were of the highest purity available unless otherwise noted and were used as received. All solvents were anhydrous and were used as received. Complete list is reported in the Supporting Information.

QD Synthesis. All QDs were synthesized in a three-neck flask connected to a standard Schlenk line setup under oxygen- and water-free conditions. Details on the synthetic procedures are given in the Supporting Information.

Synthesis of $\text{ArCS}_2^-/\text{Et}_3\text{NH}^+$. A 500 mL round-bottomed flask was filled with magnesium turnings (6.07 g, 0.500 mol) and tetrahydrofuran (THF, 5 mL) under a nitrogen atmosphere. A solution of 4-bromo-toluene (8.55 g, 0.025 mol) in THF (250 mL) was dropped into the flask with a rate of addition adjusted to maintain a gentle reflux of the resulting mixture. Upon addition of the aryl-bromide, the obtained mixture was refluxed for a further 1 h by external warming. The solution of the Grignard reagent was cooled to room temperature before addition via cannula to a flask containing carbon disulfide (11.42 g, 0.150 mol) kept at 0 °C. During the addition, the solution became reddish. The reaction was quenched by addition of diethyl-ether/water (1/1 vol/vol, 100 mL) followed by dropping concn HCl to the stirred mixture until the aqueous layer was acidic to the litmus paper. The organic layer was separated, washed with water, and dried over Na_2SO_4 . After solvent removal, the obtained crude violet product was dissolved in hexane (100 mL), and triethylamine (10 mL) was added to the mixture. After 10 min, the triethylammonium salt precipitated as a red powder, which was filtered, washed with hexane and diethyl-ether, and dried in vacuo (yield 42%). ^1H NMR (700 MHz, CDCl_3): 8.37 (d, $J = 8.2$ Hz, 2H), 7.04 (d, $J = 8.2$ Hz, 2H), 3.25 (q, $J = 7.0$ Hz, 6H), 2.33 (s, 3H), 1.39 (t, $J = 7.0$ Hz, 9H) ppm. ^{13}C NMR (176 MHz, CDCl_3): 253.1, 148.6, 140.3, 127.6, 127.0, 46.0, 21.2, 8.6 ppm. Spectra are shown in the Supporting Information (Figures S1 and S2).

UV–Vis–NIR Absorption Spectroscopy. The optical absorption spectra of colloidal QDs were measured in quartz cuvettes with 1 cm path length or on glass slides and were recorded with a Varian Cary 5000 UV–vis–NIR spectrophotometer. Spectrophotometric titration experiments were performed by adding microliter aliquots of the

replacing ligand solutions to micromolar dichloromethane solutions of colloidal QDs in a quartz cuvette. Molar absorption coefficients, ϵ , of the investigated ligand/QD systems were estimated using the Lambert–Beer law ($A = \epsilon b[\text{QD}]$, where A is the absorbance and b is the optical path length) and previously reported calculations relating ϵ and diameter values for PbS QDs.⁹ The validity of these estimations relies on the linearity of the measured absorbance with the concentration of PbS QDs in dichloromethane solution (as shown in Figure S3, Supporting Information) and on the independence of absorption coefficient at 400 nm with PbS QD size (Figure S4, Supporting Information),⁹ which implies that pristine long-chain aliphatic ligands, such as oleylamine(Cl^-) (and oleate, we assumed), may not markedly affect PbS QD absorption at 400 nm.

Fourier Transform Infrared Spectroscopy (FTIR). FTIR measurements in the 4000–400 cm^{-1} spectral range were carried out on samples deposited on silicon substrates using a Jasco FT/IR 6300 spectrophotometer apparatus operating in transmission mode at a resolution of 4 cm^{-1} .

Nuclear Magnetic Resonance Spectroscopy (NMR). ^1H and ^{13}C NMR spectra of samples in CDCl_3 or $\text{C}_6\text{D}_5\text{CD}_3$ solutions with concentrations ranging between 0.1 and 1 mM were recorded on a 700 MHz Bruker Avance instrument at 298 K.

Inductively Coupled Plasma Atomic Emission Spectroscopy (ICP-AES). ICP-AES measurements were performed with a Varian 720-ES spectrometer. The samples for the analyses were prepared by digesting dried QD powders in concentrated HNO_3 .

Transmission Electron Microscopy (TEM). TEM images were recorded with a Jeol Jem 1011 microscope operated at an accelerating voltage of 100 kV. Samples for analysis were prepared by dropping a QD solution onto carbon-coated Cu grids and then allowing the solvent to evaporate in vapor controlled environment.

Computational Methodology. We have carried out atomistic simulations at the density functional theory (DFT) level using the PBE exchange-correlation functional²² and the def2-SV(P) basis set.^{23,24} Scalar relativistic effects were incorporated by employing on the Pb atoms the Stuttgart RSC Segmented/ECP basis set with 60 core electrons.²⁵ All structures have been optimized in the gas phase, and the nature of all stationary points (in this case minima on the potential energy surface) was confirmed by normal-mode analysis. Details on the PbS model are given in the text. All calculations were carried out using the Turbomole 6.6 package.²⁶ Time-dependent calculations were carried out using the recently developed simplified Tamm–Danoff (sTDA) approach,²⁷ which allows the computation of thousands of excited states in one simple run. This methodology is suitable to compute the optical absorption spectrum of the ligand/cluster systems employed in this work until 3.5 eV. The localized orbitals of the ligand or the inorganic core have been computed separately in the field generated by the other and have been computed according to previous reports.^{28,29} Briefly, we localized the orbitals of the ligand/cluster system by block diagonalizing the Fock matrix into the orbitals of the two arbitrary subsystems (in our work the ligands and the PbS cluster). In this representation, the diagonal elements of the Fock matrix are the energies of the localized subsystems. These elements have been computed using a locally developed code. The qualitative independence of our results from the employed level of theory was demonstrated by comparing the results obtained on the formiate- and benzenethiolate–cluster model systems with the more computationally feasible PBE functional with those obtained with the computationally demanding PBE0 exchange-correlation functional (see Figure S5, Supporting Information). The density of states is similarly described with both the PBE and PBE0 functionals, with the only exception of the band gap energy, which is larger for the PBE0. On this basis, we decided to use the PBE functional, which guarantees accurate enough results with reduced calculation effort (our model ligand/cluster systems comprise up to 600 atoms). We also show that solvation effects do not markedly affect the calculated density of states of the formate/cluster system employed in this work (Figure S5, Supporting Information): indeed, the presence of a surrounding solvent (dichloromethane, as in the optical absorption measurements) barely affects the calculated density of states. For this reason, all

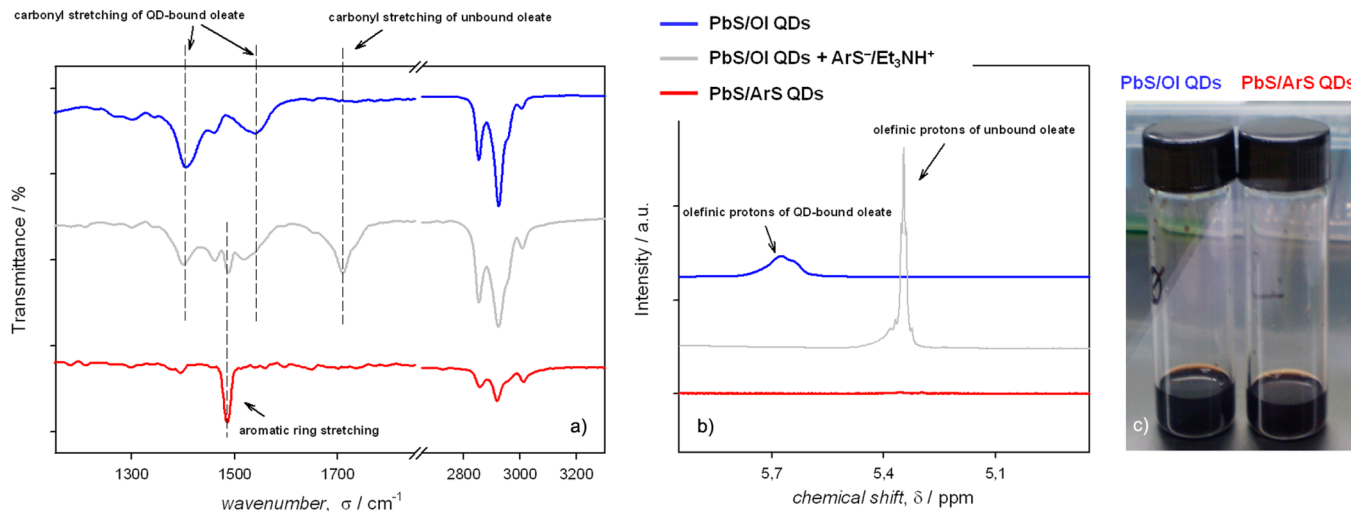


Figure 1. (a) FTIR spectra of solids of PbS/OI QDs (blue line), PbS/OI QDs upon addition of 250 equiv of $\text{ArS}^-/\text{Et}_3\text{NH}^+$ (gray line), and purified PbS/ArS QDs (red line). (b) ^1H NMR spectra of 0.1 mM solutions of PbS/OI QDs (in $\text{C}_6\text{D}_5\text{CD}_3$, blue line), PbS/OI QDs upon addition of 250 equiv of $\text{ArS}^-/\text{Et}_3\text{NH}^+$ (in CDCl_3 , gray line), and purified PbS/ArS QDs (in CDCl_3 , red line). Spectra have been vertically offset for clarity and spectral features accounting for quantitative oleate displacement have been marked. Breaks have been inserted to highlight such relevant spectral features. Complete FTIR and ^1H NMR spectra are shown in Figure S6, Supporting Information. (c) Daylight picture of three-month old 0.1 mM solutions of PbS/OI QDs (left) and PbS/ArS QDs (right). Corresponding optical absorption spectra are shown in Figure S7, Supporting Information.

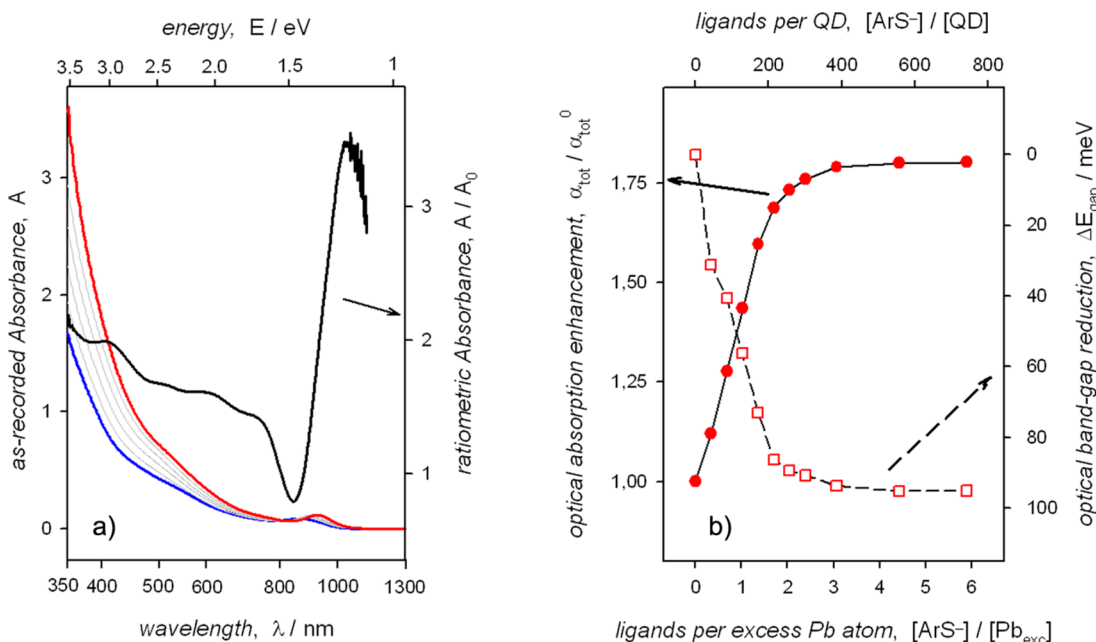


Figure 2. (a) Absorbance spectra of a $1.8 \mu\text{M}$ dichloromethane solution of colloidal PbS/OI QDs (blue line), upon addition of $\text{ArS}^-/\text{Et}_3\text{NH}^+$ (gray lines) up to about 750 equiv (red line); black line highlights spectral dependence of the broadband optical absorption enhancement observed at the plateau of the titration of colloidal PbS/OI QDs with $\text{ArS}^-/\text{Et}_3\text{NH}^+$. (b) Plots of the broadband optical absorption enhancement ($\alpha_{\text{tot}}/\alpha_{\text{tot}}^0$, full circles) and of optical band gap reduction (ΔE_{gap} , empty squares) upon addition of $\text{ArS}^-/\text{Et}_3\text{NH}^+$ to PbS/OI QDs in dichloromethane solution; lines are guide to the eye only.

structures were computed in gas phase without the inclusion of solvent effects.

RESULTS AND DISCUSSION

Quantitative Solution-Phase Ligand Exchange. The addition of $\text{ArS}^-/\text{Et}_3\text{NH}^+$ to dichloromethane solution of oleate-capped PbS QDs³⁰ (henceforth referred to as PbS/OI QDs) induces the displacement of pristine oleate ligands from the QD surface, presumably as $\text{O}^-/\text{Et}_3\text{NH}^+$ ionic couple, as

suggested by FTIR spectra, which show the appearance of the stretching vibration of carbonyl moieties of uncoordinated oleate molecules (around 1700 cm^{-1} , gray line in Figure 1a). Complete oleate displacement is demonstrated by the disappearance of carboxylate peaks in FTIR spectra and by the presence of the aromatic ring stretching peculiar to ArS^- (at $\sim 1500 \text{ cm}^{-1}$, red line in Figure 1a) as a result of the purification, which involves quantitative precipitation with excess hexane and redispersion in chlorinated solvents. The

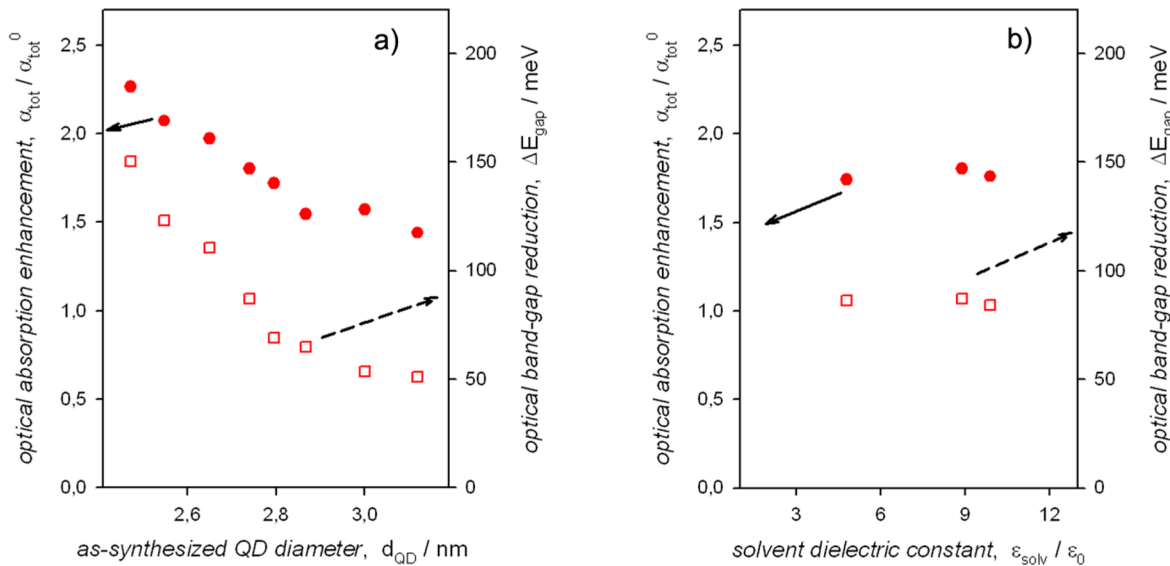


Figure 3. (a) Plots of the broadband optical absorption enhancement ($\alpha_{\text{tot}} / \alpha_{\text{tot}}^0$, full circles) and of the optical band gap reduction (ΔE_{gap} , empty squares) upon complete oleate exchange with ArS^- species at the surface of PbS QDs in dichloromethane solution as a function of as-synthesized QD diameter, d_{QD} . (b) Plots of the broadband optical absorption enhancement ($\alpha_{\text{tot}} / \alpha_{\text{tot}}^0$, full circles) and of the optical band gap reduction (ΔE_{gap} , empty squares) upon complete oleate exchange with ArS^- species at the surface of PbS QDs as a function of solvent dielectric constant, $\epsilon_{\text{solv}} / \epsilon_0$ (from left to right, chloroform, dichloromethane, and *o*-dichlorobenzene).

effective precipitation of ligand exchanged PbS/ArS QDs with hexane also qualitatively accounts for efficient replacement of oleate ligands: indeed, hexane is a good solvent for PbS/OI QDs, while it is not for PbS/ArS QDs; hence less apolar solvents have to be used in order to dissolve PbS/ArS QDs, such as dichloromethane (or chloroform, dichlorobenzene). Further confirmation of the quantitative oleate displacement is provided by ^1H NMR spectrum of PbS/OI QDs upon addition of $\text{ArS}^-/\text{Et}_3\text{NH}^+$, which displays resonance of oleate olefinic protons as a sharp multiplet at lower chemical shifts compared with the broad peak at ~ 5.7 ppm peculiar to oleate molecules bound to QDs (compare blue and gray lines in Figure 1b).^{31,32} Successive precipitation of PbS QDs with excess hexane and redispersion in CDCl_3 leads to the disappearance of olefinic proton resonance in ^1H NMR spectrum (red line, Figure 1b), again accounting for the quantitative replacement of pristine oleate ligands from the QD surface.

Optical Absorption Enhancement. The addition of $\text{ArS}^-/\text{Et}_3\text{NH}^+$ to PbS/OI QDs in dichloromethane solution induces a large optical absorption increase across the entire UV-vis-NIR spectral range ($\lambda > 350$ nm) and a bathochromic shift of the first excitonic peak (Figure 2a). We have already reported this experimental observation in a previous study,¹⁶ and here we further extend its description and explanation. The optical absorption spectrum undergoes a sudden modification upon simple mixing of the two components (PbS QDs and ArS⁻ ligands) in a closed system (a quartz cuvette) at room temperature, without any further handling of the samples, such as filtering or transferring, thus controlling QD concentration. The modified absorption spectrum is constant with time and does not show any light scattering ascribable to aggregation, as demonstrated by the negligible extinction of the incident light at energies below the first excitonic peak (i.e., $\lambda > 1000$ nm). Furthermore, the observed broadband absorption enhancement (expressed as $\alpha_{\text{tot}} / \alpha_{\text{tot}}^0$, where $\alpha_{\text{tot}} = \int \epsilon(\nu) d\nu$ integrated below 3.5 eV and α_{tot}^0 is the same parameter determined for the as-synthesized PbS/OI QDs; see Experimental Section for details

on ϵ calculations) and the optical band gap reduction (denoted as $\Delta E_{\text{gap}} = E_{\text{gap}}^0 - E_{\text{gap}}$) reach a plateau at a given ArS^- to QD molar ratio, beyond which the absorption spectrum does not appreciably change, suggesting that the PbS QD surface is no longer accessible to extra added ArS^- ligands (see Figure 2b). In order to correlate such a saturation effect to the extent of QD surface modification, we determined in analogy with previous reports the excess of Pb atoms (Pb_{ex}).^{33,34} Elemental analysis (by ICP-AES) reveals a Pb-to-S molar ratio of 1.8 for as-synthesized PbS/OI QDs, thus implying that observed optical absorption changes reach a plateau upon the addition of two ArS^- ligands per excess Pb atom (see Figure 2b and Supporting Information for calculation details);³⁵ moreover, ICP-AES yields a Pb/S molar ratio of 0.66 upon $\text{ArS}^-/\text{Et}_3\text{NH}^+$ addition supporting the presence of two ArS^- ligands per excess Pb atom in the ligand-exchanged PbS/ArS QDs sample.

The observed spectral changes could, in principle, be trivially explained by the addition of absorbing species or by an increase of the QD size. However, the ArS^- ligands show an absorption onset around 300 nm (see absorption spectra of all the replacing ligands employed in this work in Figure S8, Supporting Information) and the observation of a plateau upon subsequent addition of $\text{ArS}^-/\text{Et}_3\text{NH}^+$ clearly points to the negligible contribution of the ligand absorption to spectral changes observed below 3.5 eV (or above 350 nm). The growth of the QDs is unlikely to occur in the mild experimental conditions (room temperature) of our solution-phase ligand exchange process; although the diameter changes corresponding to the observed red-shift of the first excitonic peak⁹ would correspond to about 0.2 nm (roughly one-third of the PbS lattice constant) and therefore are highly difficult to experimentally verify, any PbS formation could be optically detected (gray spectrum in Figure S9, Supporting Information) upon addition of $\text{ArS}^-/\text{Et}_3\text{NH}^+$ to Pb(II)-oleate, even upon heating at 110 °C, the temperature at which PbS QDs have been synthesized, in accordance with previous reports.³⁶ The broadband absorbance increase and the red shift of the first

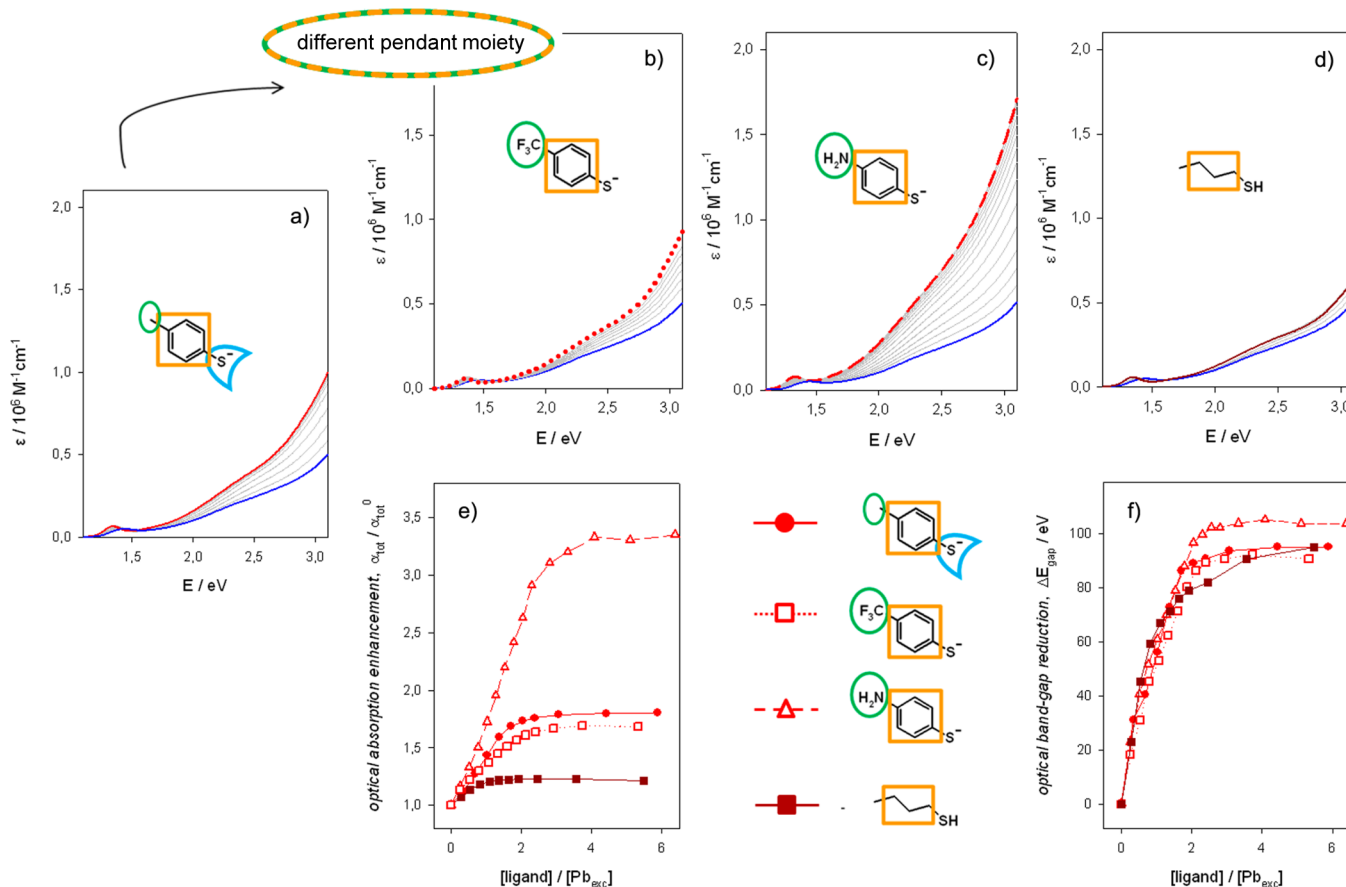


Figure 4. (a–d) Optical absorption spectra of dichloromethane solution of PbS/OI QDs (blue spectra) upon addition of (a) $\text{ArS}^-/\text{Et}_3\text{NH}^+$, (b) $\text{A-ArS}^-/\text{Et}_3\text{NH}^+$, (c) $\text{D-ArS}^-/\text{Et}_3\text{NH}^+$, and (d) AlSH. Colored lines represent the spectra obtained at the plateau of the titration experiments. (e,f) Plots of the corresponding broadband optical absorption enhancement ($\alpha_{\text{tot}} / \alpha_{\text{tot}}^0$, panel e) and of the optical band gap reduction (ΔE_{gap} , panel f) as a function of the number of replacing ligands added per excess Pb atoms on the QD surface. Lines have been drawn to guide the eye only. Symbols representing each replacing ligand appear between $\alpha_{\text{tot}} / \alpha_{\text{tot}}^0$ and ΔE_{gap} plots.

excitonic peak are instead markedly dependent on QD surface-to-volume ratio: indeed, the larger the QD diameter, the smaller the $\alpha_{\text{tot}} / \alpha_{\text{tot}}^0$ and the ΔE_{gap} as represented in Figure 3a by full and empty symbols, respectively. The extent of ArS^- ligand effect on the absorption spectrum of colloidal PbS QDs increases with increasing QD surface-to-volume ratio, therefore implying an effect exerted at the ligand/QD interface. Furthermore, such an effect is barely influenced by the dielectric constant of the surrounding solvent medium, as shown in Figure 3b.

The Role of the Ligand Pendant Moiety. In order to evaluate the replacing ligand effect on the optical absorption properties of strongly quantum-confined PbS QDs with diameter of about 3 nm, we have systematically modified pendant and anchoring moieties of the arenethiolate ligand framework (as shown in Scheme 1). Hence we have investigated whether the presence of electronically active substituents in the para position of the benzenethiolate framework (see Scheme 1) may further affect optical absorption of colloidal PbS QDs. In presence of the electron-withdrawing trifluoromethyl group as for $\text{A-ArS}^-/\text{Et}_3\text{NH}^+$, the optical absorption increase (upon addition to PbS/OI QDs in dichloromethane solution) is slightly lower than that induced by the addition of ArS^- ligands, while a comparable bathochromic shift of the first excitonic peak is observed (Figure 4b and empty squares in Figure 4e,f); as for ArS^-

ligands, the spectral changes reach a plateau upon the addition of two A-ArS^- ligands per Pb_{exc} suggesting an analogously efficient coordination of PbS QD surface. Conversely, in the presence of the electron-donor amino group as for $\text{D-ArS}^-/\text{Et}_3\text{NH}^+$, a much larger optical absorption enhancement can be achieved, whereas comparable ΔE_{gap} again accounts for a similar stoichiometry of the ligand exchanged species (Figure 4c and empty triangles in Figure 4e,f). Noticeably, the replacement of the conjugated moiety linked to the thiolate anchoring group with a saturated chain, as for AlSH, is accompanied by a slight absorption increase, while the ΔE_{gap} is analogous to that induced by aromatic thiolates (Figure 4d and full squares in Figure 4e,f). These findings clearly show that conjugated thiolate ligands drastically increase broadband optical absorption of colloidal PbS QDs, which can be tuned and further enhanced by suitable electronically active substituents; such an enhancement is observed in a broad spectral range (at energies below 3.5 eV), thus comprising the high energy region (above 3.1 eV or below 400 nm) for which it has been previously found that (molar) absorption coefficient is not affected by quantum confinement.⁹

In order to further investigate the origin of the observed ligand-induced spectral changes, we performed density functional theory (DFT) calculations on a nonstoichiometric model for the PbS inorganic core, formally a $(\text{Pb}_{55}\text{S}_{38})^{34+}$ cluster, which displays a Pb/S ratio of 1.45 and a cuboctahedral shape.

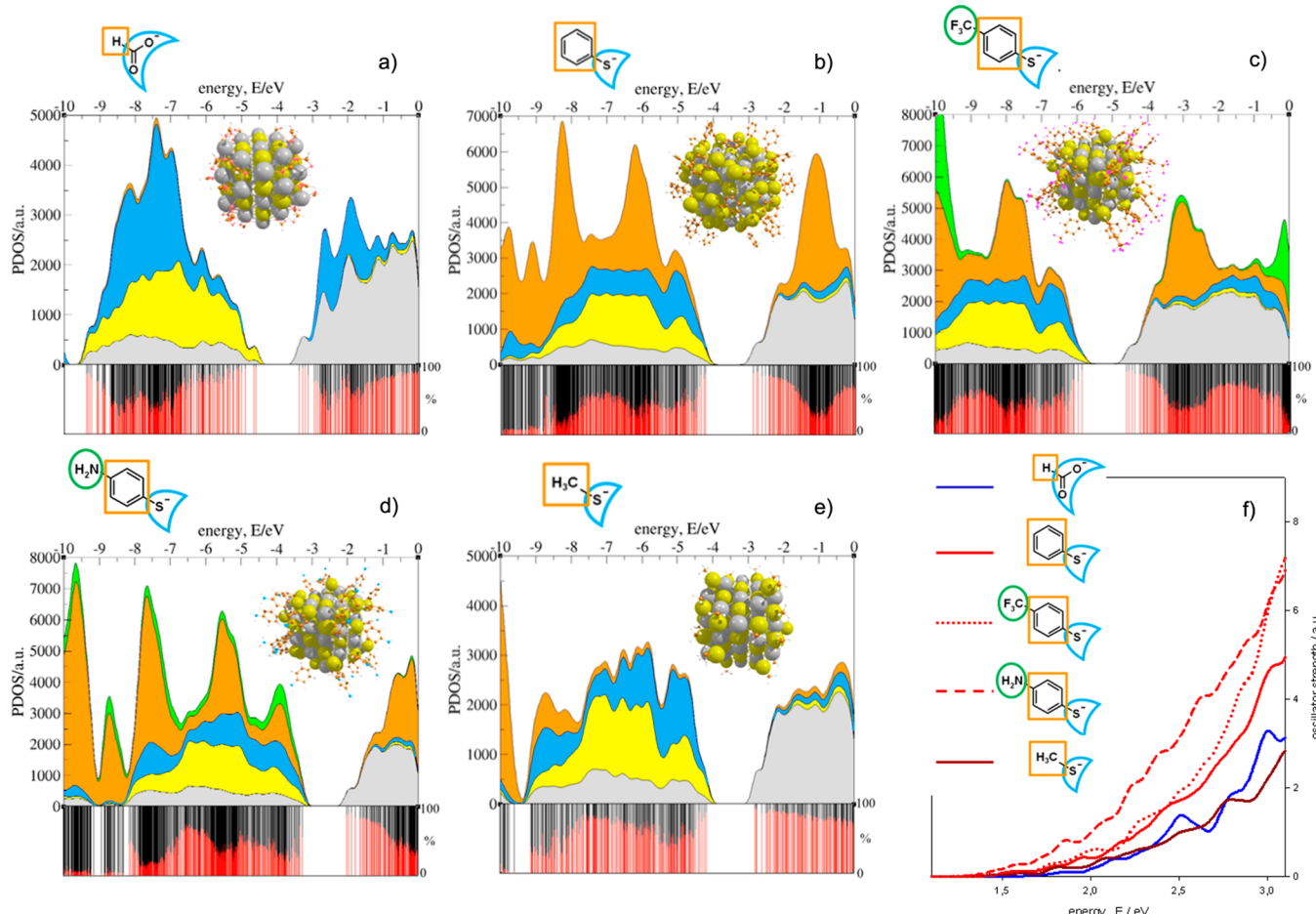


Figure 5. (a–e) Projected density of states (PDOS) resulting from DFT calculations of the model $(\text{Pb}_{55}\text{S}_{38})^{34+}$ clusters capped with 34 anionic ligands, namely, (a) Fo^- , (b) PhS^- , (c) A-ArS^- , (d) D-ArS^- , and (e) MeS^- , which have been chosen in analogy to experimentally used ligands Ol^- , ArS^- , A-ArS^- , D-ArS^- , and AlSH , respectively. At the bottom of each PDOS plot appears the contribution of both ligands (in black) and inorganic cluster (in red) to the orbitals of the entire ligand/cluster system. Minimized ligand/QD model structures and ligands are shown in the corresponding PDOS panels. Pb orbitals of the inorganic cluster are shown in gray, S orbitals of the inorganic cluster in yellow, orbitals localized on the anchoring group of the ligand in cyan, orbitals localized on the backbone of ligand's pendant group in orange, and orbitals localized on the substituents of the ligand's pendant group in green, according to colors used to represent ligand/cluster structures. (f) Corresponding TDDFT calculated absorption spectra; legend appears on the left side of the panel.

Charge neutrality in the model is kept by adding 34 anionic organic species, representing Ol^- , ArS^- , A-ArS^- , D-ArS^- , and AlS^- ligands bound to external Pb^{II} atoms, mostly at the $\langle 111 \rangle$ facets (see Supporting Information for optimized structures, Figures S11–15). The feasibility of this model has been recently proposed.³⁷ Such model systems aim at uncovering the role of the pendant benzene ring (or aliphatic chain) bearing electronically active substituents on the density of states of our ligand/QD systems. The projected density of states (PDOS in Figure 5a–e) clearly shows the relevant contribution of benzene orbitals to the density of states of the corresponding ligand/QD systems, together with the involvement of 3p orbitals of the S anchoring atom in the highest occupied ligand/QD states (whereas O anchoring atoms provide a minor contribution). By time-dependent DFT (TDDFT) calculations, performed with the same relaxed structure, functional, and basis set as the ground state ones, we calculated the optical absorption spectra displayed in Figure 5f. This shows a drastic increase of the oscillator strength in the presence of the benzene ring, which is further enhanced by the para-substituted amino group. The absence of the conjugated pendant moiety does not induce appreciable absorption enhancement, in

agreement with experimental observations. Despite the good agreement with experimental observations concerning the relative absorption intensities, our ligand/cluster models do not exactly reproduce the thiolate-induced band gap reduction. The reasons for such discrepancy are currently under investigation and may presumably be linked to the large quantum confinement effects that are taking place in small ligand/cluster systems as those presented in this work and to the eventual distortion of such small clusters induced by coordinated ligands. In this regard, preliminary calculations clearly show relevant fluctuations of the band gap energies for small clusters bearing different ligands (see Figure S16, Supporting Information), which might be at the basis of the discrepancy between experiment and computation. Nevertheless, this limitation of our model does not affect its validity for the purpose of this work: indeed, the enhanced absorption intensity, which derives from the mixing between the organic ligand and the inorganic core orbitals, is computationally ascertained rather independently from the employed level of theory, the inclusion of solvation effects, and the size of the computed clusters (see Experimental Section and Supporting Information). DFT calculations also suggest that replacing

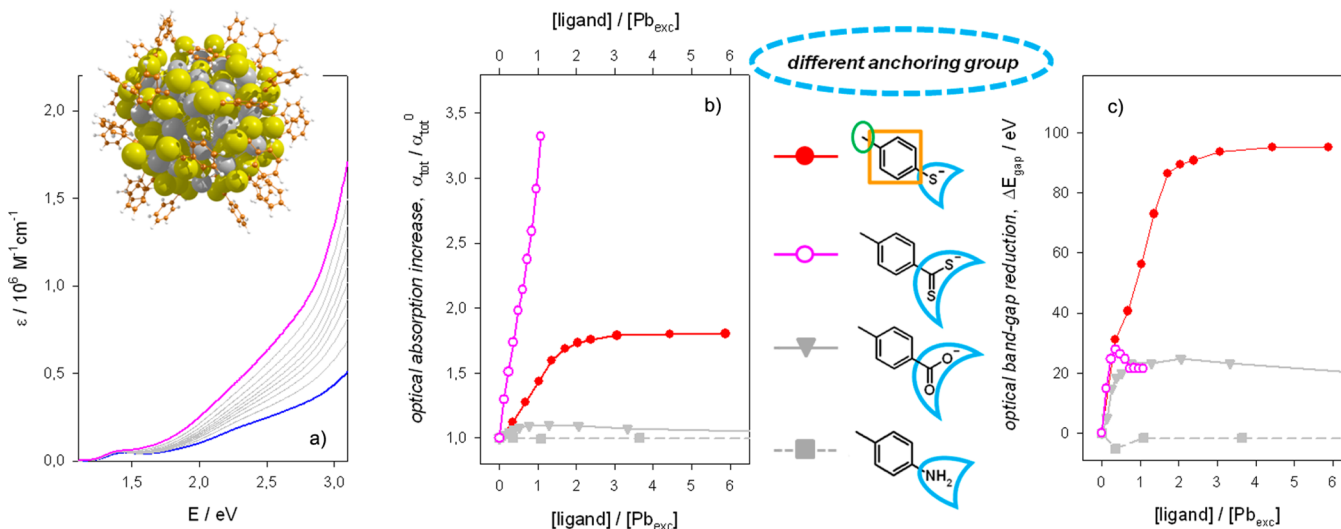


Figure 6. (a) Optical absorption spectra of dichloromethane solution of PbS/OI QDs (blue spectrum) upon addition of ArCS₂⁻/Et₃NH⁺. Purple line represents the spectrum obtained at the end of the titration experiments. Optimized structure of the calculated Pb₅₅S₃₈(PhCS₂)₃₄ is shown, suggesting inorganic cluster distortion upon ligand binding. (b,c) Plots of the corresponding broadband optical absorption enhancement ($\alpha_{\text{tot}}/\alpha_{\text{tot}}^0$, panel b) and of the optical band gap reduction (ΔE_{gap} , panel c) as a function of the number of replacing ligands added per excess Pb atoms on QD surface. Lines have been drawn to guide the eye only. Symbols representing replacing ligands are drawn between $\alpha_{\text{tot}}/\alpha_{\text{tot}}^0$ and ΔE_{gap} plots.

ligands may shift the band energies of corresponding ligand/QD systems, in analogy to recent observation on PbS QD solids.⁴ Indeed, with the addition of electronically active substituents in the para position of the benzenethiolate ligands, DFT calculations clearly show that withdrawing electrons from the PbS cluster (with A-ArS⁻ ligands, Figure 5c) lowers band energies of the entire ligand/cluster systems, whereas pushing electron density toward the PbS cluster (with D-ArS⁻ ligands, Figure 5d) raises absolute band energies. This computationally inferred finding suggests the possibility to gain control of ionization potential and electron affinity of QDs via organic ligands, which could be experimentally substantiated by photoelectron spectroscopic measurements.

DFT calculations are qualitatively consistent with the experimentally observed optical absorption enhancement, thus accounting for strong ligand/QD electronic interactions. Conversely, the absorption onset of the employed thiolate ligands (≥ 3.5 eV) excludes that the light absorption increase could be trivially attributed to their contribution, whereas polarization effect (or solvatochromism) is expected to barely affect optical absorption spectra, as shown by changing the dielectric constant of the surrounding medium (Figure 3b); moreover, with a two-level nearly free electron model³⁸ to describe the first excitonic transition of our inorganic core/ligand shell/solvent medium system (see Supporting Information for details, pages S18–20), the polarization effect induced by the replacing the ligand shell negligibly affects both the local electric field^{39,40} and the energy of the optical band gap.^{41,42} Indeed, DFT calculations suggest that orbitals localized on the conjugated thiolate ligands largely contribute to the density of states of the ligand/QD system. This is corroborated by calculating the contribution of organic and inorganic components to the entire ligand/cluster orbitals, which shows that orbital mixing is involved in essentially every electronic state of the ligand/QD system (see the bottom part of panels a–e in Figure 5). Therefore, coupling of QD localized orbitals with partially mixed π orbitals of the benzene ring and nonbonding orbitals localized on the S anchoring atom⁴³ leads to broad increase of the number of allowed transitions, thus

inducing the observed optical absorption enhancement. The optical absorption enhancement could be in principle explained also by an increase of the oscillator strengths of weak or dark transitions induced by conjugated thiolates. In this regard, the analysis of the calculated electronic transitions for formate- and benzenethiolate-capped (Pb₅₅S₃₈)³⁴⁺ clusters (see Figure S17, Supporting Information) clearly shows that the broadband density of allowed transitions is significantly improved, whereas an increase of the oscillator strength may occur in proximity of the band gap. The contribution from 3p orbitals localized on the sulfur anchoring atom to the density of the highest occupied states is instead, most likely, responsible for the optical band gap reduction.

The Role of Ligand Anchoring Group. We have thus modified the binding moiety on the *p*-methylbenzene group of the replacing ligands in order to elucidate the role exerted by the chemical nature and bonding mode of the anchoring groups on the optical absorption properties of colloidal PbS QDs. To this aim, we have synthesized *p*-methylbenzenedithioate ligands as triethylammonium salt (ArCS₂⁻/Et₃NH⁺). Upon addition of such bidentate S-terminated ligand to PbS/OI QD solutions in the same experimental conditions as previously discussed for monodentate thiolate ligands, we observe a much larger absorbance increase for the same number of added replacing ligands (Figure 6a and empty circles in Figure 6b), although resulting QDs show poorer colloidal stability. We notice that ArCS₂⁻ addition induces a smaller bathochromic shift of the first excitonic peak compared with ArS⁻ ligands and that the plot of ΔE_{gap} reaches a plateau for only one ArCS₂⁻ ligand per Pb_{exc} (empty circles in Figure 6c); we can expect that charge neutrality is guaranteed by other anionic species not displaced from the QD surface, and in this regard, it is worth mentioning that previous reports on PbS/OI QDs obtained with similar synthetic procedure have demonstrated the presence of one oleate ligand per Pb_{exc} while charges are balanced by OH⁻ anions produced during lead(II)-oleate homoleptic complex formation.⁴⁴ The saturation effect observed for one ArCS₂⁻ ligand per Pb_{exc} and the concomitant poor colloidal stability of the resulting species may result from the large strain induced on

PbS QDs by ArCS_2^- ligands as suggested by DFT calculation (structure of corresponding cluster $\text{Pb}_{55}\text{S}_{38}(\text{PhCS}_2)_3$ is shown on top of Figure 6a and in the Supporting Information with the corresponding PDOS plot) and from the eventual steric hindrance of bidentate ligands. Furthermore, addition of bidentate O-terminated ligands $\text{ArCO}_2^-/\text{Et}_3\text{NH}^+$ leads to slight spectral changes (which again reach a plateau for one ArCO_2^- ligand per Pb_{exc} ; full triangles in Figure 6b,c), whereas addition of N-terminated ligands, ArNH_2 , does not induce appreciable spectral changes (full squares in Figure 6b,c), which can be ascribed to poor QD surface coordination; neutral ArNH_2 ligands are expected to replace $\text{Pb}^{II}(\text{Ol})_2$ complexes from the QD surface,^{31,37} and the lack of a hypsochromic shift observed accounts for weak coordination to the PbS QD surface, whereas ArCO_2^- ligands may partially displace pristine oleate ligands since aromatic carboxylates are weaker and more polarizable bases than aliphatic carboxylates. Conversely, the soft character of S-terminated bases leads to more stable coordination interactions with Pb^{II} cations, thus implying that the amino group of D- ArS^- ligand does not appreciably contribute to or alter the coordination to QD surface, which is therefore expected to occur exclusively via the thiolate moiety.

On the Absorption Coefficient of Colloidal PbS QDs at High Energies. The systematic investigation of the ligand effect on the optical absorption properties of colloidal PbS QDs clearly shows that S-terminated ligands bearing a conjugated moiety induce a large absorbance increase, which is particularly relevant at high energies (above 3.1 eV, or below 400 nm) where it has been previously reported that the molar absorption coefficient ($\epsilon_{400\text{nm}}$; or the per particle cross section, $\sigma_{400\text{nm}}$) is not affected by quantum confinement.^{9,39} Generally, optical transitions far from the band gap occurring in dilute dispersions of colloidal QDs have been modeled within the framework of effective medium theory, which yields absorption coefficients at energies far from the band gap that linearly scale with nanocrystal volume.^{6–9} The validity of this approximation implies a density of states that approaches a continuum and the absence of strong resonances. Our work shows that such an approximation largely fails to estimate the optical absorption of small PbS QDs (where small stands for large surface-to-volume ratio) coordinated by conjugated S-terminated ligands (see Figure 7).

Indeed, we calculate $\epsilon_{400\text{nm}}$ values that are up to 340% larger than those previously reported for colloidal PbS QDs with diameters of about 3 nm (see Table 1), which are particularly relevant for photovoltaic applications.^{45,46} Such $\epsilon_{400\text{nm}}$ values are larger for bidentate conjugated dithioate ligands (ArCS_2^-) compared with monodentate conjugated thiolates (ArS^-) for the same number of added replacing ligands, whereas slight $\epsilon_{400\text{nm}}$ increase is induced by saturated thiols (AlSH). This observation points out the significance of the π character of the entire replacing ligand on the QD optical absorption properties, which can be tuned and further enhanced via electron-donating substituents (as for D- ArS^-) increasing the electron density of the organic shell. On this basis, we suggest that organic ligands are inherently coupled to the inorganic cores in colloidal QDs, thus resulting in optical properties that cannot be expected to coincide with those estimated by using formalisms derived from light scattering of small particles that include bulk parameters.

According to DFT calculations (see above), the conjugated S-terminated ligands coordinated to the PbS QD surface broadly increase the number of allowed transitions of the resulting ligand/QD system via orbital mixing of the organic

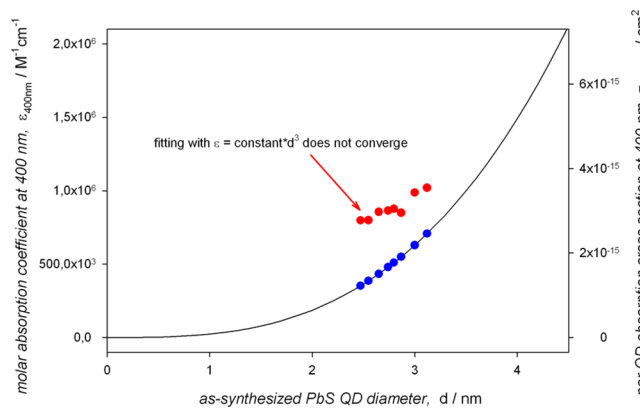


Figure 7. Molar absorption coefficient, ϵ , and per particle cross section, σ , at 400 nm of as-synthesized PbS/OI QDs (blue circles) estimated according to calculations derived from effective medium theory (black line).⁹ Molar absorption coefficient at 400 nm of PbS/ArS QDs (red circles) estimated by using the Lambert–Beer law for titration experiments in a closed system.

Table 1. Values of Molar Absorption Coefficient at 400 nm ($\epsilon_{400\text{nm}}$), Broadband Optical Absorption Increase ($\alpha_{\text{tot}}/\alpha_{\text{tot}}^0$), and Optical Bandgap Reduction (ΔE_{gap}) Obtained for Colloidal PbS QDs in the Presence of 400 equiv of the Ligands (i.e., at the Plateau of the Titration Experiments) Shown in the Library of Scheme 1^a

ligand at PbS QD surface	$\epsilon_{400\text{nm}} \times 10^6 \text{ M}^{-1} \text{ cm}^{-1}$	$\alpha_{\text{tot}}/\alpha_{\text{tot}}^0$	$\Delta E_{\text{gap}} \text{ (meV)}$
ArS^-	1.0	1.8	92
A- ArS^-	0.93	1.7	90
D- ArS^-	1.7	3.3	100
AlS ⁻	0.64	1.2	92
ArCS_2^- ^b	1.7 (1.3 ^c)	3.3 (2.9 ^c)	22
ArCO_2^-	0.58	1.1	24
ArNH_2	0.51	1.0	0.0

^aAll values have been determined assuming that $\epsilon_{400\text{nm}} = 0.51 \times 10^6 \text{ M}^{-1} \text{ cm}^{-1}$ for PbS/OI QDs with a diameter of 2.8 nm (see Experimental Section for details).⁹ ^bValues obtained upon addition of 130 equiv of $\text{ArCS}_2^-/\text{Et}_3\text{NH}^+$ ligands due to the poor colloidal stability of the resulting system. ^cValues in parentheses were obtained by subtracting the contribution of $\text{ArCS}_2^-/\text{Et}_3\text{NH}^+$ ligand to the absorption spectrum.

and inorganic components. The resulting chemical species display peculiar properties that cannot be described as the mere sum of those of the ligand and QD components: indeed, this clearly emerges by comparing the calculated orbitals for the entire ligand/cluster system with the orbitals of ligands and clusters experiencing each other's electric field (see Figure 8) and by analyzing ratiometric and differential absorption spectra (shown in Figure S23, Supporting Information). The QD surface-to-volume ratio dependence of the observed optical absorption increase (empty circles in Figure 3a) becomes extremely large in the strong quantum confinement regime experienced by small QDs,⁴⁷ and therefore these two effects cannot be straightforwardly disentangled. The ligand/QD systems here investigated thus require a refined model beyond effective medium theory to describe and eventually predict their optical absorption properties.

On the Origin of the Excitonic Red-Shift Commonly Observed for Thiol-Treated PbS QD Solids. The replacement of the bulky electrically insulating ligands coming

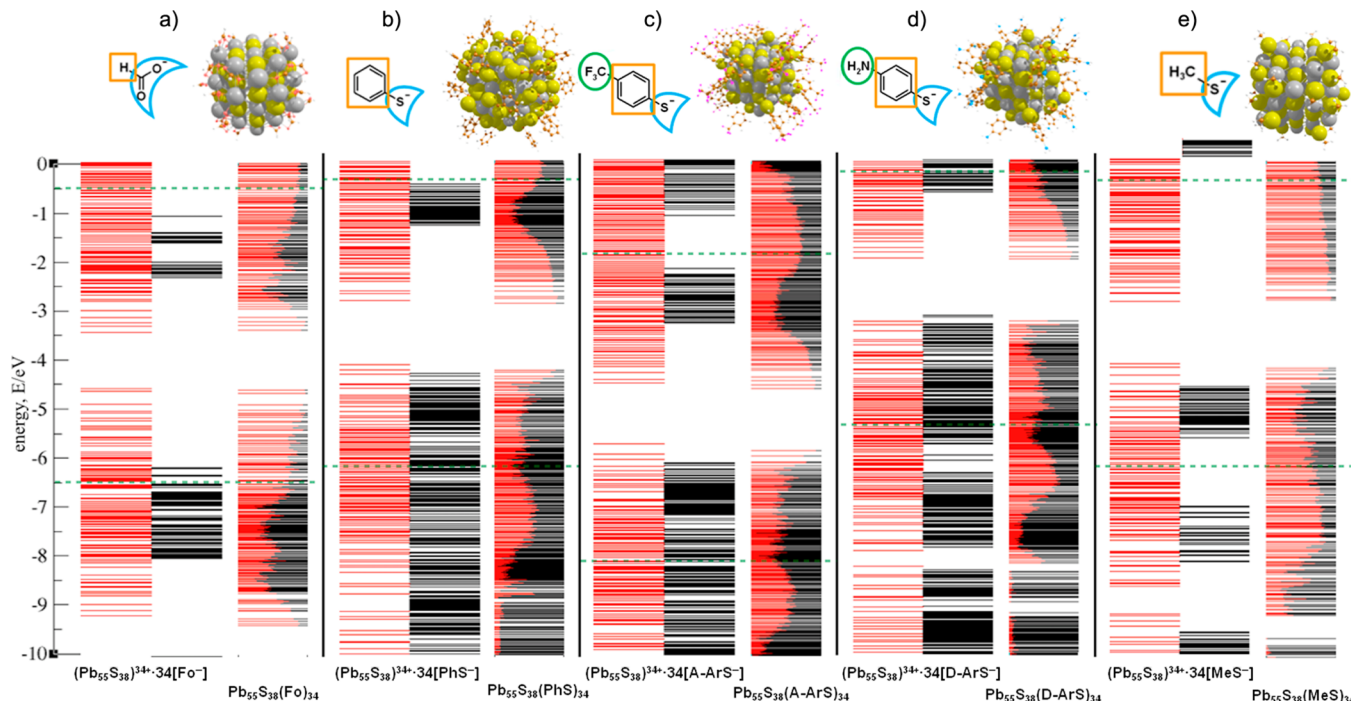


Figure 8. Calculated ligand/cluster orbitals for the model $(\text{Pb}_{55}\text{S}_{38})^{34+}$ clusters capped with 34 anionic ligands, namely (a) FO^- , (b) PhS^- , (c) ArS^- , (d) D-ArS^- , and (e) MeS^- , which have been chosen in analogy to experimentally used ligands Ol^- , ArS^- , A-ArS^- , D-ArS^- , and AlSH , respectively, showing the contribution of organic ligands (in black) and inorganic core (in red). Orbitals appearing with mixed red and black color on the right side of each panel are delocalized orbitals of the entire ligand/cluster system (denoted as $\text{Pb}_{55}\text{S}_{38}(\text{ligand})_{34}$), in which the intensity of each color defines the contribution of either the ligand or the core to a given orbital. The orbitals on the left side represent contribution of ligands (black) and core (red) experiencing each other's electric field (referred to as $(\text{Pb}_{55}\text{S}_{38})^{34+}\cdot 34[\text{ligand}^-]$), that is, the electronic structure of each fragment has been constructed by considering charge rearrangement only within each fragment (induced by the presence of the other fragment) and not between fragments (charge transfer between them). In other words, the orbitals on the left side (red + black) provide the electronic structure of the overall ligand/cluster system in the case of pure ionic interaction between the inorganic and organic parts. Dashed green lines limit the range of orbitals contributing to the calculated optical absorption spectra shown in Figure 5f below 3.5 eV. Minimized ligand/QD model structures and ligands are shown on top of the corresponding orbital panels.

from the synthetic procedure with short chemical species is mandatory for effective QD-based optoelectronic applications. Pristine ligand replacement in solution phase presents relevant advantages compared with commonly employed solid-phase ligand exchange because it (i) ensures complete access of the replacing ligands to the QD surface thus favoring a quantitative ligand exchange process, (ii) reduces the formation of trap states by allowing a more efficient elimination of side products, and (iii) permits the deposition of the QD-based active layers in a single step thus overcoming the wasteful layer-by-layer approach usually employed in device fabrication.^{16,48,49} In addition, solution-phase ligand exchange allows us to (iv) investigate the ligand/QD interactions on isolated species and discriminate the concomitant inter-QD interactions occurring when ligands are exchanged in solid phase. In this regard, we have already shown that thiolate-terminated ligands induce a noticeable optical band gap reduction when added to PbS/OI QD solutions. Such a reduction does not depend on the nature of the appended moieties (aromatic or aliphatic, the former bearing electronically active substituents; see Figure 4f). This has been attributed to 3p orbitals localized on the S anchoring atom, which contribute to higher occupied states of the resulting ligand/QD systems, and we therefore propose that it can account for most of the bathochromic shift commonly observed after the postdeposition treatment of lead-chalcogenide QD solids with short thiol-terminated (saturated and conjugated) molecules.⁵⁰ Indeed, the addition in solution phase

of ArS^- ligands to PbS/OI QDs with diameter of 2.8 nm induces a bathochromic shift of the first excitonic peak of about 90 meV, whereas solids obtained upon deposition on a glass substrate of purified PbS/ArS QDs show an optical band gap reduction of about 100 meV compared with solids of corresponding PbS/OI QDs (Figure 9). On this basis, we propose that the optical band gap reduction in PbS/ArS QD solids may be prevalently (~90%) ascribed to the contribution of S 3p orbitals of the thiol ligands to the higher occupied states of the QDs: this effect is exerted on isolated QDs by the coordinated thiolates already before deposition; therefore we refer to it as intra-QD exciton delocalization. The extra red-shift observed in solid phase (~10%) instead arises from interactions between adjacent QDs and can be thus attributed to inter-QD exciton delocalization (or excitonic coupling, dipole–dipole coupling), whereas inter-QD electronic coupling can be regarded as negligible due the low field-effect mobility observed in PbS/ArS QD solids,¹⁶ according to the Einstein–Smoluchowski relation. Our description of the first excitonic peak red shift commonly observed upon the postdeposition treatment of lead-chalcogenide QD solids with thiols relies on the successful attainment of colloidal thiolate-capped PbS QDs that are free-standing in solution phase and then self-assemble thereof, which allow us to discriminate between intra- and inter-QD interactions, whereas solid-phase ligand exchange hinders such a distinction. Other mechanisms already envisaged to explain the ligand-induced red shift of the first excitonic peak

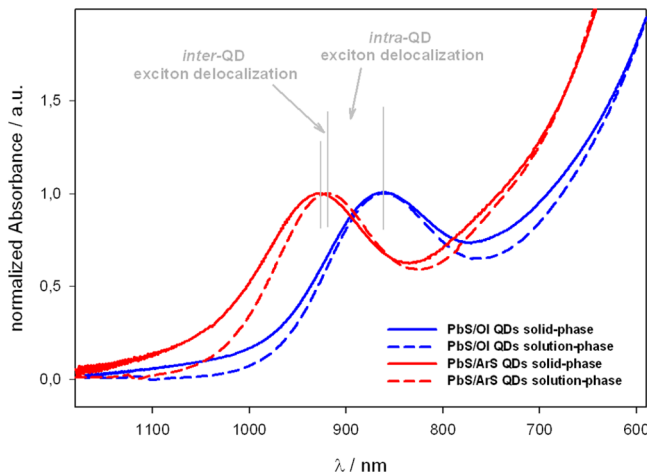


Figure 9. Optical absorption spectra of solution-phase (dashed lines) and solid-phase (solid lines) PbS/OI QDs (blue lines) and PbS/ArS QDs (red lines) normalized at the maximum of the first excitonic peak. Vertical gray lines have been drawn to emphasize the bathochromic shift of the first excitonic peak occurring upon solution-phase ligand exchange of PbS/OI QDs to PbS/ArS QDs and then to solids thereof.

in PbS QD solids are not applicable to our system. For instance, exciton delocalization on the ligand shell previously attributed to the resonance between the highest occupied states of the QDs and the ligands is not appropriate to our systems since it was inferred by estimating QD and ligand energy levels as distinct entities from bulk values and DFT calculations, respectively (Figure S24, Supporting Information, shows the energy level diagram obtained for our system by using this approach);¹⁸ moreover, a refined version of this model suggests that the ligand-induced optical band gap reduction depends on the energy of the HOMO level of ligands,⁵¹ while we observe analogous red shift induced by thiolate-terminated ligands regardless of the nature of the pendant moieties (see Figure 4) and despite the marked shift of their HOMO levels. Further explanation based on quantum-confined Stark effect⁵² is unlikely since the ligand-induced red shift would be expected to increase for larger QDs,⁵³ while we observe the opposite dependence (Figure 3a). Furthermore, our results point out that previously proposed replacing ligand-induced polarization effect,⁵⁴ or solvatochromism, can be considered negligible as demonstrated by poor spectral dependence on dielectric constant of the solvent (Figure 3b) and by calculations based on effective medium approximation (see Supporting Information).

CONCLUSION

In this study, we have described a novel design concept for light-harvesting nanomaterials to be applied in solution-processed photovoltaic and photodetection applications. Indeed, we have demonstrated that suitable QD surface modification with short conjugated organic molecules permits enhancement (>300%) of broadband light absorption of PbS QDs, while preserving good long-term colloidal stability. Such a design concept is based on the evidence that organic ligands and inorganic cores constituting the colloidal semiconductor nanocrystals are inherently electronically coupled materials; therefore rational design of the organic shell gives rise to ligand/QD species displaying enhanced optical absorption properties that could not be predicted on the basis of isolated

ligand and QD components. Here we have provided systematic investigation of ground-state ligand/QD interactions leading to such a drastic enhancement of broadband optical absorption and described the prominent role exerted by the chemical nature and coordination geometry of the anchoring group and its π conjugation with the pendant moiety, which mediate the electronic coupling with the PbS QD cores. We note that qualitatively similar optical absorption changes are observed upon addition of ArS⁻/Et₃NH⁺ to oleate-capped CdS QDs⁵⁵ (see Figure S25, Supporting Information), thus suggesting possible general applicability of the principles here presented and described. Conversely, the absorption spectra of colloidal CdS and CdSe/CdS core/(elongated)shell QDs capped with aliphatic phosphine oxide and phosphonic acid ligands⁵⁶ are slightly affected by arenethiolate ligands (see Figure S25, Supporting Information). As already discussed, carboxylates rather weakly coordinate large, highly polarizable Pb^{II} and Cd^{II} cations and therefore are easily replaced by thiolate-terminated ligands, whereas phosphine oxide- and phosphonic acid-based ligands, commonly considered as soft bases, are expected to stably bind Cd atoms at the QD surface and therefore are less easily replaced by thiolates. These findings result in a simple and effective approach to enhance and tune broadband solar-light absorption of colloidal metal-chalcogenide QDs, which could be exploited for the design of light-harvesting systems to be applied for solution-processed photovoltaic and photodetection applications; the employed short ligands reduce inter-QD distance in solids^{16,17} and may eventually further increase optical absorption via dipolar coupling,⁵⁷ representing a relevant contribution to the optimization of photoactive QD layer thickness, which affects absorption of the incident light and transport of photogenerated charges thus ultimately mediating photon-to-charge carrier conversion efficiencies.

ASSOCIATED CONTENT

Supporting Information

Details on the synthesis of colloidal QDs, further spectrophotometric characterization of ligands and QDs, TEM images of QDs, and details on DFT and effective medium approximation calculations. This material is available free of charge via the Internet at <http://pubs.acs.org>.

AUTHOR INFORMATION

Corresponding Author

*carlo.giansante@iit.it

Notes

The authors declare no competing financial interest.

ACKNOWLEDGMENTS

We thank L. Carbone and G. Lerario for fruitful discussion. This work was supported by Progetto di ricerca PON R&C 2007-2013 (Avviso n. 713/Ric. del 29 ottobre 2010) MAAT-Molecular Nanotechnology for Health and Environment (Project Number: PON02_00563_3316357), Regione Puglia (APQ-Reti di Laboratorio, Project PHOEBUS, cod. 31-FE1.20001), EFOR-Energia da FOnti Rinnovabili (Iniziativa CNR per il Mezzogiorno L. 191/2009 art. 2 comma 44), and by the European project ESCORT- Efficient Solar Cells based on Organic and hybrid Technology (seventh FWP - reference number 261920). IvInf thanks the Department of Industry of the Basque Country (grant SAIOTEK S-PC12UN003) and the

SGI/IZO-SGIker UPV/ EHU for generous allocation of computational resources.

■ REFERENCES

- (1) Kim, J. Y.; Voznyy, O.; Zhitomirsky, D.; Sargent, E. H. *Adv. Mater.* **2013**, *25* (36), 4986–5010.
- (2) Yin, Y.; Alivisatos, A. P. *Nature* **2005**, *437* (7059), 664–670.
- (3) Talapin, D. V.; Lee, J.-S.; Kovalenko, M. V.; Shevchenko, E. V. *Chem. Rev.* **2010**, *110* (1), 389–458.
- (4) Brown, P. R.; Kim, D.; Lunt, R. R.; Zhao, N.; Bawendi, M. G.; Grossman, J. C.; Bulović, V. *ACS Nano* **2014**, *8* (6), 5863–5872.
- (5) Fischer, S. A.; Crotty, A. M.; Kilina, S. V.; Ivanov, S. A.; Tretiak, S. *Nanoscale* **2012**, *4* (3), 904–914.
- (6) Leatherdale, C. A.; Woo, W. K.; Mikulec, F. V.; Bawendi, M. G. *J. Phys. Chem. B* **2002**, *106* (31), 7619–7622.
- (7) Yu, P.; Beard, M. C.; Ellington, R. J.; Ferrere, S.; Curtis, C.; Drexler, J.; Luiszer, F.; Nozik, A. J. *J. Phys. Chem. B* **2005**, *109* (15), 7084–7087.
- (8) Moreels, I.; Lambert, K.; De Muynck, D.; Vanhaecke, F.; Poelman, D.; Martins, J. C.; Allan, G.; Hens, Z. *Chem. Mater.* **2007**, *19* (25), 6101–6106.
- (9) Moreels, I.; Lambert, K.; Smeets, D.; De Muynck, D.; Nollet, T.; Martins, J. C.; Vanhaecke, F.; Vantomme, A.; Delerue, C.; Allan, G.; Hens, Z. *ACS Nano* **2009**, *3* (10), 3023–3030.
- (10) Konstantatos, G.; Howard, I.; Fischer, A.; Hoogland, S.; Clifford, J.; Klem, E.; Levina, L.; Sargent, E. H. *Nature* **2006**, *442* (7099), 180–183.
- (11) Hinds, S.; Levina, L.; Klem, E. J. D.; Konstantatos, G.; Sukhovatkin, V.; Sargent, E. H. *Adv. Mater.* **2008**, *20* (23), 4398–4402.
- (12) Law, M.; Luther, J. M.; Song, Q.; Hughes, B. K.; Perkins, C. L.; Nozik, A. J. *J. Am. Chem. Soc.* **2008**, *130* (18), 5974–5985.
- (13) Gao, Y.; Aerts, M.; Sandeep, C. S. S.; Talgorn, E.; Savenije, T. J.; Kinge, S.; Siebbeles, L. D. A.; Houtepen, A. J. *ACS Nano* **2012**, *6* (11), 9606–9614.
- (14) Dong, A.; Ye, X.; Chen, J.; Kang, Y.; Gordon, T.; Kikkawa, J. M.; Murray, C. B. *J. Am. Chem. Soc.* **2010**, *133* (4), 998–1006.
- (15) Fafarman, A. T.; Koh, W.-k.; Diroll, B. T.; Kim, D. K.; Ko, D.-K.; Oh, S. J.; Ye, X.; Doan-Nguyen, V.; Crump, M. R.; Reifsnider, D. C.; Murray, C. B.; Kagan, C. R. *J. Am. Chem. Soc.* **2011**, *133* (39), 15753–15761.
- (16) Giansante, C.; Carbone, L.; Giannini, C.; Altamura, D.; Ameer, Z.; Maruccio, G.; Lojudice, A.; Belviso, M. R.; Cozzoli, P. D.; Rizzo, A.; Gigli, G. *J. Phys. Chem. C* **2013**, *117* (25), 13305–13317.
- (17) Giansante, C.; Carbone, L.; Giannini, C.; Altamura, D.; Ameer, Z.; Maruccio, G.; Lojudice, A.; Belviso, M. R.; Cozzoli, P. D.; Rizzo, A.; Gigli, G. *Thin Solid Films* **2014**, *560*, 2–9.
- (18) Frederick, M. T.; Amin, V. A.; Cass, L. C.; Weiss, E. A. *Nano Lett.* **2011**, *11* (12), 5455–5460.
- (19) Fischer, A.; Rollny, L.; Pan, J.; Carey, G. H.; Thon, S. M.; Hoogland, S.; Voznyy, O.; Zhitomirsky, D.; Kim, J. Y.; Bakr, O. M.; Sargent, E. H. *Adv. Mater.* **2013**, *25* (40), 5742–5749.
- (20) Danehy, J. P.; Parameswaran, K. N. *J. Chem. Eng. Data* **1968**, *13* (3), 386–389.
- (21) Masui, M.; Sayo, H.; Tsuda, Y. *J. Chem. Soc. B* **1968**, 973–976.
- (22) Perdew, J. P.; Burke, K.; Ernzerhof, M. *Phys. Rev. Lett.* **1996**, *77* (18), 3865–3868.
- (23) Eichkorn, K.; Weigend, F.; Treutler, O.; Ahlrichs, R. *Theor. Chem. Acta* **1997**, *97* (1–4), 119–124.
- (24) Weigend, F.; Ahlrichs, R. *Phys. Chem. Chem. Phys.* **2005**, *7* (18), 3297–3305.
- (25) Metz, B.; Stoll, H.; Dolg, M. *J. Chem. Phys.* **2000**, *113* (7), 2563–2569.
- (26) Furche, F.; Ahlrichs, R.; Hättig, C.; Klopper, W.; Sierka, M.; Weigend, F. *Wiley Interdiscip. Rev.: Comput. Mol. Sci.* **2014**, *4* (2), 91–100.
- (27) Grimme, S. *J. Chem. Phys.* **2013**, *138* (24), No. 244104.
- (28) Kondov, I.; Čížek, M.; Benesch, C.; Wang, H.; Thoss, M. *J. Phys. Chem. C* **2007**, *111* (32), 11970–11981.
- (29) Li, J.; Wang, H.; Persson, P.; Thoss, M. *J. Chem. Phys.* **2012**, *137* (22), No. 22A529.
- (30) Hines, M. A.; Scholes, G. D. *Adv. Mater.* **2003**, *15* (21), 1844–1849.
- (31) Anderson, N. C.; Hendricks, M. P.; Choi, J. J.; Owen, J. S. *J. Am. Chem. Soc.* **2013**, *135* (49), 18536–18548.
- (32) Gomes, R.; Hassinen, A.; Szczęgiel, A.; Zhao, Q.; Vantomme, A.; Martins, J. C.; Hens, Z. *J. Phys. Chem. Lett.* **2011**, *2* (3), 145–152.
- (33) Moreels, I.; Fritzinger, B.; Martins, J. C.; Hens, Z. *J. Am. Chem. Soc.* **2008**, *130* (45), 15081–15086.
- (34) Hughes, B. K.; Ruddy, D. A.; Blackburn, J. L.; Smith, D. K.; Bergren, M. R.; Nozik, A. J.; Johnson, J. C.; Beard, M. C. *ACS Nano* **2012**, *6* (6), 5498–5506.
- (35) Jasieniak, J.; Mulvaney, P. *J. Am. Chem. Soc.* **2007**, *129* (10), 2841–2848.
- (36) Shaw, R. A.; Woods, M. *J. Chem. Soc. A* **1971**, 1569–1571.
- (37) Sandeep, C. S. S.; Azpiroz, J. M.; Evers, W. H.; Boehme, S. C.; Moreels, I.; Kinge, S.; Siebbeles, L. D. A.; Infante, I.; Houtepen, A. J. *ACS Nano* **2014**, *8* (11), 11499–11511.
- (38) Brus, L. E. *J. Chem. Phys.* **1984**, *80* (9), 4403–4409.
- (39) Hens, Z.; Moreels, I. *J. Mater. Chem.* **2012**, *22* (21), 10406–10415.
- (40) Neeves, A. E.; Birnboim, M. H. *J. Opt. Soc. Am. B* **1989**, *6* (4), 787–796.
- (41) Leatherdale, C. A.; Bawendi, M. G. *Phys. Rev. B* **2001**, *63* (16), No. 165315.
- (42) Allan, G.; Delerue, C.; Lannoo, M.; Martin, E. *Phys. Rev. B* **1995**, *52* (16), 11982–11988.
- (43) Aoki, M.; Kamada, T.; Sasaki, K.; Masuda, S.; Morikawa, Y. *Phys. Chem. Chem. Phys.* **2012**, *14* (12), 4101–4108.
- (44) Zhrebetsky, D.; Scheele, M.; Zhang, Y.; Bronstein, N.; Thompson, C.; Britt, D.; Salmeron, M.; Alivisatos, P.; Wang, L.-W. *Science* **2014**, *344* (6190), 1380–1384.
- (45) Ning, Z.; Voznyy, O.; Pan, J.; Hoogland, S.; Adinolfi, V.; Xu, J.; Li, M.; Kirmani, A. R.; Sun, J.-P.; Minor, J.; Kemp, K. W.; Dong, H.; Rollny, L.; Labelle, A.; Carey, G.; Sutherland, B.; Hill, I.; Amassian, A.; Liu, H.; Tang, J.; Bakr, O. M.; Sargent, E. H. *Nat. Mater.* **2014**, *13* (8), 822–828.
- (46) Chuang, C.-H. M.; Brown, P. R.; Bulović, V.; Bawendi, M. G. *Nat. Mater.* **2014**, *13* (8), 796–801.
- (47) Wise, F. W. *Acc. Chem. Res.* **2000**, *33* (11), 773–780.
- (48) Ning, Z.; Dong, H.; Zhang, Q.; Voznyy, O.; Sargent, E. H. *ACS Nano* **2014**, *8* (10), 10321–10327.
- (49) Giansante, C.; Mastria, R.; Lerario, G.; Moretti, L.; Kriegel, I.; Scotognella, F.; Lanzani, G.; Carallo, S.; Esposito, M.; Biasiucci, M.; Rizzo, A.; Gigli, G. *Adv. Funct. Mater.* **2015**, *25*, 111–119.
- (50) Choi, J. J.; Luria, J.; Hyun, B.-R.; Bartnik, A. C.; Sun, L.; Lim, Y.-F.; Marohn, J. A.; Wise, F. W.; Hanrath, T. *Nano Lett.* **2010**, *10* (5), 1805–1811.
- (51) Frederick, M. T.; Amin, V. A.; Swenson, N. K.; Ho, A. Y.; Weiss, E. A. *Nano Lett.* **2012**, *13* (1), 287–292.
- (52) Yaacobi-Gross, N.; Soreni-Harari, M.; Zimin, M.; Kababya, S.; Schmidt, A.; Tessler, N. *Nat. Mater.* **2011**, *10* (12), 974–979.
- (53) Wen, G. W.; Lin, J. Y.; Jiang, H. X.; Chen, Z. *Phys. Rev. B* **1995**, *52* (8), 5913–5922.
- (54) Wolcott, A.; Doyeux, V.; Nelson, C. A.; Gearba, R.; Lei, K. W.; Yager, K. G.; Dolocan, A. D.; Williams, K.; Nguyen, D.; Zhu, X. Y. *J. Phys. Chem. Lett.* **2011**, *2* (7), 795–800.
- (55) Yu, W. W.; Peng, X. *Angew. Chem., Int. Ed.* **2002**, *41* (13), 2368–2371.
- (56) Carbone, L.; Nobile, C.; De Giorgi, M.; Sala, F. D.; Morello, G.; Pompa, P.; Hytch, M.; Snoeck, E.; Fiore, A.; Franchini, I. R.; Nadasan, M.; Silvestre, A. F.; Chiodo, L.; Kudera, S.; Cingolani, R.; Krahne, R.; Manna, L. *Nano Lett.* **2007**, *7* (10), 2942–2950.
- (57) Geiregat, P.; Justo, Y.; Abe, S.; Flamee, S.; Hens, Z. *ACS Nano* **2013**, *7* (2), 987–993.